

Generalized Gilat-Raubenheimer method for density-of-states calculation in photonic crystals

Boyuan Liu¹, Steven G. Johnson², John D. Joannopoulos³, Ling Lu¹

¹Institute of Physics, Chinese Academy of Sciences/Beijing National Laboratory for Condensed Matter Physics, Beijing 100190, China

²Department of Mathematics, Massachusetts Institute of Technology, Cambridge, Massachusetts 02139, USA

³Department of Physics, Massachusetts Institute of Technology, Cambridge, Massachusetts 02139, USA

E-mail: linglu@iphy.ac.cn

Abstract.

Efficient numeric algorithm is the key for accurate evaluation of density of states (DOS) in band theory. Gilat-Raubenheimer (GR) method proposed in 1966 is an efficient linear extrapolation method which was limited in specific lattices. Here, using an affine transformation, we provide a new generalization of the original GR method to any Bravais lattices and show that it is superior to the tetrahedron method and the adaptive Gaussian broadening method. Finally, we apply our generalized GR (GGR) method to compute DOS of various gyroid photonic crystals of topological degeneracies.

Keywords: density of states, photonic crystal, topological photonics

1. Introduction

Numerical methods of DOS calculations [1] fall into two categories, extrapolation and interpolation. Each category can use linear or high-order fittings. Linear extrapolation methods include GR [2, 3, 4, 5, 6] and adaptive (Gaussian) broadening [7]. The high-order extrapolation methods were discussed in [8, 9]. Linear interpolation methods include the tetrahedron method [10, 11, 12], which does not need group-velocity information and is flexible in terms of volume grid division into tetrahedrons. The high-order interpolation methods were discussed in reference [13, 14, 15].

The extrapolation methods are better than the interpolation methods at band crossings [8, 16]. The interpolation methods interpolate the frequency (or energy) data from the nearest-neighbor momenta for linear interpolations and requires more neighboring data points for high-order interpolations. At the band crossings, interpolation methods sample the points across the degeneracy, resulting in the increase of errors. In contrast, an extrapolation method extrapolates the neighboring frequency data using both the frequency and the group velocity (first derivative) at each momentum point for linear extrapolations and requires higher-order derivatives for high-order extrapolations. Consequently, the extrapolation methods are not vulnerable to the band crossings while the interpolation methods are.

GR is the first linear extrapolation method proposed. It was originally formulated in the three-dimensional (3D) cubic grid and was extended to hcp [3], tetragonal [4] and trigonal lattices [5], by dividing the irreducible Brillouin zones (IBZ) into rectangular and triangular prisms. An improved GR method [6] derives the analytical formulation of the DOS contribution for parallelepiped subcells, applicable to all Bravais lattices. In this work, using a geometric transformation between a cube and a parallelepiped, we made a simpler generalization of the original GR method for all lattices. The convergence plots show that our GGR method is consistently more accurate than the commonly-used tetrahedron and Gaussian methods. In Appendix A, we showed that this GGR method is equivalent to the improved GR method derived in a different way. In Appendix B, we discussed the GGR method for 2D.

In photonics, GR method has never been adopted. Tetrahedron method [17] and histogramming [18, 19, 20] were used instead. A new method named Dirichlet-to-Neumann maps [21] has been implemented in 2D photonic crystals for finding both the DOS and the equifrequency surfaces. In this paper, we applied the GGR method to photonic crystals.

The rest of the paper is arranged in the following

way. Section 2 introduced the details of this transformation for our GGR method. Section 3 compared the convergence of different methods. In section 4, we applied our method to topological photonic crystals. Section 5 discussed the computing efficiency of the GGR method. Section 6 concluded our findings.

2. Generalizing GR method by affine transformation

The core idea of our GGR method is to use an affine transformation [6] to transform a parallelepiped BZ into a cube, so that the original GR method can be used for any lattice. The BZ is a parallelepiped constituted by three reciprocal vectors \mathbf{b}_i ($i = 1, 2, 3$), starting from an arbitrary point \mathbf{k}_0 . The \mathbf{k} points are uniformly distributed along three basis vectors \mathbf{b}_i . The affine transformation changes the \mathbf{k} -basis of the parallelepiped BZ into $\mathbf{t} = (t_1, t_2, t_3)$ of a cubic volume,

$$\mathbf{k} - \mathbf{k}_0 = B\mathbf{t} = \mathbf{b}_1 t_1 + \mathbf{b}_2 t_2 + \mathbf{b}_3 t_3, \quad (1)$$

where $t_1, t_2, t_3 \in [0, 1]$ and $B = [\mathbf{b}_1, \mathbf{b}_2, \mathbf{b}_3]$. Consequently the volume elements of the two sets of bases satisfies $dV_k = \det(B)dV_t = \Omega dV_t$, in which Ω is the volume of the BZ.

We convert the DOS $[D(\omega)]$, the integral on equifrequency surface S_ω , from the \mathbf{k} basis into the cubic \mathbf{t} basis

$$D(\omega) = \frac{1}{\Omega} \sum_n \int_{S_\omega} \frac{dS_k}{|\mathbf{v}_k|} = \sum_n \int_{S_\omega} \frac{dS_t}{|\mathbf{v}_t|}, \quad (2)$$

since

$$\frac{1}{\Omega} \frac{dS_k dk_\perp}{|\mathbf{v}_k| dk_\perp} = \frac{1}{\Omega} \frac{dV_k}{d\omega} = \frac{dV_t}{d\omega} = \frac{dS_t dt_\perp}{|\mathbf{v}_t| dt_\perp}, \quad (3)$$

where \mathbf{v}_k and \mathbf{v}_t are the group velocities in each basis and k_\perp and t_\perp are the vectors normal to S_ω . n is the band index. \mathbf{v}_t is obtained by scaling \mathbf{v}_k :

$$\mathbf{v}_t = \nabla_t \omega(\mathbf{k}(\mathbf{t})) = \nabla_k \omega \cdot \nabla_t (B\mathbf{t}) = \mathbf{v}_k \cdot B, \quad (4)$$

where $\mathbf{v}_k \cdot B$ is a vector whose i th component is $(\mathbf{v}_k \cdot \mathbf{b}_i)$.

So far we have transformed the integral in parallelepiped BZ into integral in cubic volume $t_i \in [0, 1]$. Then we can use original GR method to calculate the DOS in the basis of t_i . The GR method partitions the cubic integral volume into uniform small cubes, with the \mathbf{k} points at their centers. In each cubic subcell, we use linear extrapolation based on the frequency and group velocity of the central point to approximate the frequency of other region. In this case, the equifrequency surface of a given frequency is a polygon in each cubic cell. The area of the polygon is provided by the original GR method [2]. The final GGR formula is given in equation A.4 in the Appendix.

The integral region of our method is the whole BZ, a parallelepiped spanned by $\mathbf{b}_1, \mathbf{b}_2, \mathbf{b}_3$ or a fraction of

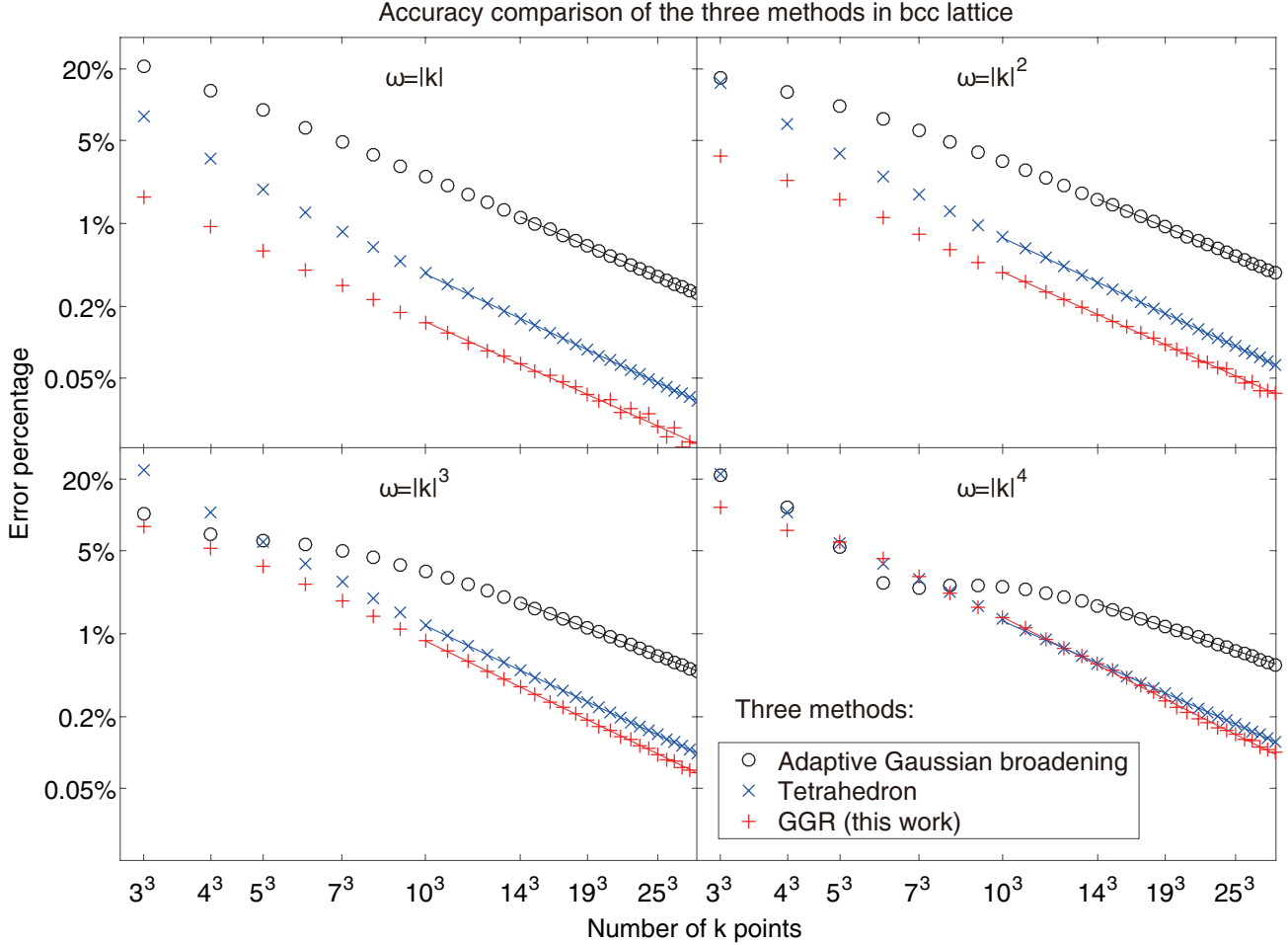


Figure 1. $error(N)$ of the three methods in bcc lattice in double-logarithmic plots. We assume that the band dispersion are $\omega = |\mathbf{k}|, |\mathbf{k}|^2, |\mathbf{k}|^3, |\mathbf{k}|^4$ respectively. The data we adopt to line fitting is from $N = 10^3$ to 32^3 for GGR and tetrahedron method and is from $N = 15^3$ to 32^3 for adaptive Gaussian broadening method. We note that the accuracy of tetrahedron method will be even worse in actual band structures with band crossings.

it. This works for the general case for all lattices and symmetries. Although using IBZ is computationally more efficient, the choice of IBZ is symmetry specific. For example, we broke both the spatial and time-reversal symmetries in section 4, and the corresponding IBZ varies from case to case. When sampling the whole BZ, we recommend that the \mathbf{k} mesh be shifted away from the BZ center (Γ) to avoid the divergence problem due to the zero group velocities [2].

3. Accuracy comparison between three methods

We compared the accuracy of GGR method with that of adaptive Gaussian broadening method and tetrahedron method. We assume that the lattice is body-centered cubic (bcc) and the BZ is a parallelepiped formed by three reciprocal lattice vectors \mathbf{b}_i ($i = 1, 2, 3$ and $|\mathbf{b}_i| = 1$) starting from origin.

The total number of \mathbf{k} points is $N = N_1 N_2 N_3$, where N_i is the number of \mathbf{k} points along \mathbf{b}_i direction, and for simplicity, we set $N_1 = N_2 = N_3$. The band frequency is $\omega = |\mathbf{k}|, |\mathbf{k}|^2, |\mathbf{k}|^3, |\mathbf{k}|^4$ respectively, so that we have analytical DOS to compare with. The error percentage is defined as:

$$error(N) = \frac{\int_0^1 |D_N(\omega) - D_\infty(\omega)| d\omega}{\int_0^1 D_\infty(\omega) d\omega}, \quad (5)$$

where $D_N(\omega)$ is the DOS calculated on N \mathbf{k} points and $D_\infty(\omega)$ is the theoretical DOS.

In figure 1, $error(N)$ of the three methods are presented in double logarithmic plots. The GGR method is better in the four cases. It is important to point out that, in the realistic band structures with band crossings, the tetrahedron interpolation method will have an even lower accuracy [8, 16]. Therefore the GGR extrapolation method is a clear winner.

We fit the errors linearly $[\ln(error(N))] =$

$p_1 \ln(N) + p_2]$ for large number of \mathbf{k} points, where p_1 and p_2 are the real fitting parameters. The power dependences of p_1 were tabulated in table 1 for all three methods. The p_1 values of GR method are consistent with the accuracy analysis in [22] which showed $error(N) \propto N^{-2/3}$. The p_1 values of the tetrahedron method are also close to the rate of convergence in [23].

Table 1. The fitting parameters of adaptive Gaussian broadening, tetrahedron and our GGR method in figure 1.

p_1	$\omega = \mathbf{k} $	$\omega = \mathbf{k}^2$	$\omega = \mathbf{k} ^3$	$\omega = \mathbf{k}^4$
Gaussian	-0.6545	-0.6314	-0.5882	-0.5118
Tetrahedron	-0.7067	-0.7059	-0.7103	-0.6712
GGR	-0.6786	-0.6757	-0.7353	-0.7625

We wrote the GGR method according to reference [2], the adaptive Gaussian broadening method following reference [7], and the tetrahedron method following reference [10, 12]. In our program of the adaptive Gaussian broadening method, width of Gaussian function is $\alpha|\mathbf{v}_{\mathbf{k}}|\Delta k$, where Δk is the side length of a subcell. We set $\alpha = 1.0$, which is a dimensionless constant indicating the broadening level. We compared our GGR method program to the original GR method program ‘‘GRINT’’ on CPC Program Library for simple cubic lattice. Our program of tetrahedron method was compared with the program ‘‘tflovrn/ctetra’’ on github. In both methods, we got numerical consistency.

4. DOS of gyroid photonic crystals

Using the GGR method, we computed the DOS of six gyroid photonic crystals in figure 2(a-f), following the original designs from reference [24] and reference [?] in which the DOS data were not presented. The insets are the real-space geometries in bcc unit cells. The band structures were calculated using MPB [26] for the frequencies and group velocities at 15^3 uniformly-distributed \mathbf{k} points in the whole BZ.

Figure 2 (a) is the single gyroid having a large band gap. Figure 2 (b) is the double gyroid (DG) having a threefold quadratic degeneracy. The DOS around the degeneracy point, of frequency ω_0 , shows a square-root relation of $D \propto |\omega - \omega_0|^{1/2}$. Figure 2 (c) is the perturbed DG having a nodal ring. The DOS around the degeneracy line shows approximately a linear relation of $D \propto |\omega - \omega_0|$. Figure 2 (d) is the parity (\mathcal{P})-breaking DG having two pairs of Weyl points. Figure 2 (e) is the time-reversal (\mathcal{T})-breaking DG having one pair of Weyl points. Figure 2 (f) is the \mathcal{P} -breaking DG having two pairs of Weyl points of the same frequency, in which the radius of the four defect air spheres is $r = 0.09a$. The DOS around the above

Weyl points all shows a roughly quadratic relation of $D \propto |\omega - \omega_0|^2$.

5. Computing efficiency

Figure 1 shows that the extrapolative GGR method is more accurate than the interpolative tetrahedron method by utilizing the extra data of group velocities, which requires extra computing time. Fortunately, the group velocities can be efficiently computed using the Hellman-Feynmann theorem $\frac{\partial \omega_{\mathbf{k}}}{\partial k_i} = \langle U_{\mathbf{k}} | \frac{\partial \hat{H}_{\mathbf{k}}}{\partial k_i} | U_{\mathbf{k}} \rangle$, where $|U_{\mathbf{k}}\rangle$ is the periodic part of the Bloch wave function and $\hat{H}_{\mathbf{k}}$ is the Hamiltonian operator of the system. Using MPB for example, the computation time for band dispersions with and without group velocities only differ by less than 2%. We note that the total computing time is proportional to the number of \mathbf{k} points N , in which the time for computing DOS is negligible compared with the time for computing the band dispersions.

6. Conclusion

In summary, we generalized GR method to all Bravais lattices using an affine transformation, which outperforms the tetrahedron and adaptive broadening methods. Our GGR method divides BZ into parallelepipeds and such extrapolation method is advantageous in treating band crossings than interpolation methods. Future work includes high-order extrapolations [27] and more versatile sub-cell division. Our codes for the GGR and tetrahedron methods will be available for download at <https://github.com/boyuanliuoptics/DOS-calculation>.

Acknowledgments

We thank Tingtao Zhou for the initial efforts in this project and Hongming Weng and C.T. Chan for discussions. Boyuan Liu thanks Hao Lin and Qinghui Yan for their help on numerics. L.L. was supported by the National key R&D Program of China under Grant No. 2017YFA0303800, 2016YFA0302400 and by NSFC under Project No. 11721404. J.D.J. and S.G.J. was partly supported by the Army Research Office through the Institute for Soldier Nanotechnologies under contract no. W911NF-13-D-0001. S.G.J. was supported in part by the Air Force Research Laboratory under Agreement No. FA8650-15-2-5220.

Appendix A. Equivalence between GGR and improved GR method

Here we prove that our GGR method is analytically equivalent to the improved GR method in reference [6].

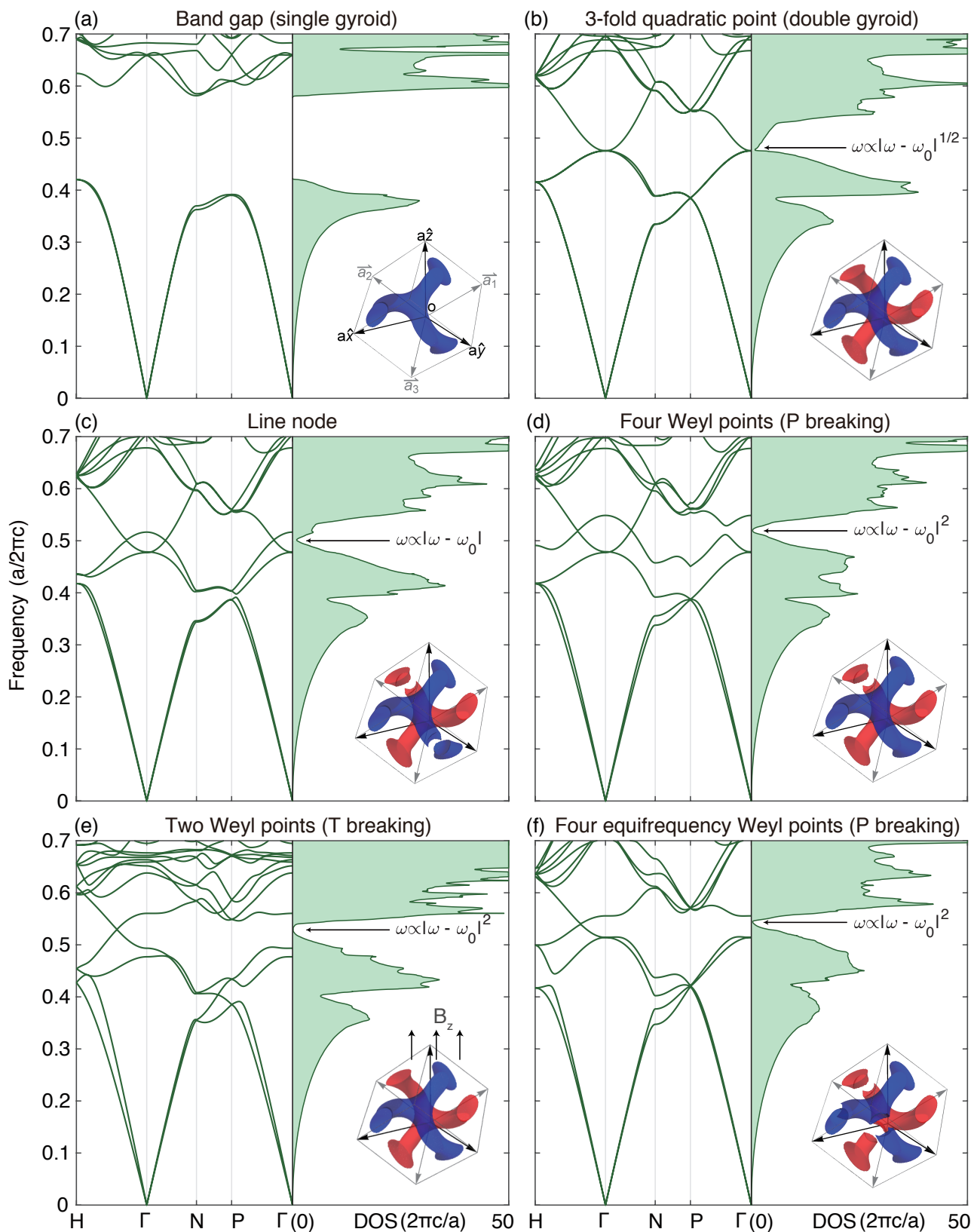


Figure 2. DOS of six gyroid photonic crystals. Gyroid photonic crystal with a band gap (a), a quadratic degeneracy point (b), a line node (c) and Weyl points (d-f). The designs of (a-e) are from reference [24] and the design of (f) is from reference [?]. Their dielectric constant is 16. Each inset shows the unit-cell geometry of the crystal whose air-sphere defects are enlarged ($0.13a$) in the illustration for the easy of identification, where a is cubic lattice constant.

In the improved GR method, the DOS contribution of one subcell is given by

$$\delta N = -\frac{1}{2} \frac{1}{B_1 B_2 B_3} \sum_{\sigma_1=0}^1 \sum_{\sigma_2=0}^1 \sum_{\sigma_3=0}^1 (-1)^{\sigma_1+\sigma_2+\sigma_3} (A - \sum_{i=1}^3 (-i)^{\sigma_i} B_i)^2 \times \theta(A - \sum_{i=1}^3 (-i)^{\sigma_i} B_i), \quad (\text{A.1})$$

where $A = \omega - \omega_c$, $B_i = \frac{1}{2} \mathbf{v} \cdot \mathbf{b}_i / N_i$ ($i = 1, 2, 3$), $\theta(x)$ is the Heaviside step function, ω_c is the frequency of central point of the subcell, \mathbf{v} is the group velocity of this subcell, \mathbf{b}_i is the reciprocal vector, N_i is the number of \mathbf{k} points along i th dimension and $N_1 = N_2 = N_3$.

In order to compare the expression (A.1) with that of our GGR method, we expand the above summation (A.1):

$$\begin{aligned} \delta N = & -\frac{1}{2} \frac{1}{B_1 B_2 B_3} \\ & \{ [A - (B_1 + B_2 + B_3)]^2 \theta(A - (B_1 + B_2 + B_3)) \\ & + [A - (B_1 - B_2 - B_3)]^2 \theta(A - (B_1 - B_2 - B_3)) \\ & + [A - (-B_1 + B_2 - B_3)]^2 \theta(A - (-B_1 + B_2 - B_3)) \\ & + [A - (-B_1 - B_2 + B_3)]^2 \theta(A - (-B_1 - B_2 + B_3)) \\ & - [A - (-B_1 - B_2 - B_3)]^2 \theta(A - (-B_1 - B_2 - B_3)) \\ & - [A - (-B_1 + B_2 + B_3)]^2 \theta(A - (-B_1 + B_2 + B_3)) \\ & - [A - (B_1 - B_2 + B_3)]^2 \theta(A - (B_1 - B_2 + B_3)) \\ & - [A - (B_1 + B_2 - B_3)]^2 \theta(A - (B_1 + B_2 - B_3)) \}. \end{aligned} \quad (\text{A.2})$$

Without loss of generality, we assume $A > 0$ and $B_1 \geq B_2 \geq B_3 \geq 0$. Then the expression (A.2) is transformed into a piecewise form,

$$\delta N = \begin{cases} \frac{B_0}{B_1} & B_1 \geq B_2 + B_3, 0 \leq A \leq A_1 \\ \frac{1}{B_1 B_2 B_3} [2(B_1 B_2 + B_2 B_3 + B_3 B_1) - (A^2 + B_0^2)] & B_1 \leq B_2 + B_3, 0 \leq A \leq A_1 \\ \frac{1}{B_1 B_2 B_3} [(B_1 B_2 + 3B_2 B_3 + B_3 B_1) - A(-B_1 + B_2 + B_3) - \frac{1}{2}(A^2 + B_0^2)] & A_1 \leq A \leq A_2 \\ \frac{2}{B_1 B_2} [(B_1 + B_2) - A] & A_2 \leq A \leq A_3 \\ \frac{1}{2B_1 B_2 B_3} [(B_1 + B_2 + B_3) - A]^2 & A_3 \leq A \leq A_4 \\ 0 & A \geq A_4 \end{cases} \quad (\text{A.3})$$

where $B_0 = (B_1^2 + B_2^2 + B_3^2)^{1/2}$, $A_1 = |B_1 - B_2 - B_3|$, $A_2 = (B_1 - B_2 + B_3)$, $A_3 = (B_1 + B_2 - B_3)$, $A_4 = (B_1 + B_2 + B_3)$.

Next, we get the expression of DOS contribution of our GGR method according to section 2,

$$\frac{dS_t}{|\mathbf{v}_t|} = \begin{cases} \frac{4b^2}{v_{t1}} & v_{t1} \geq v_{t2} + v_{t3}, 0 \leq \Delta\omega \leq \omega_1 \\ \frac{1}{v_{t1} v_{t2} v_{t3}} [2b^2(v_{t1} v_{t2} + v_{t2} v_{t3} + v_{t3} v_{t1}) - (\Delta\omega^2 + (v_t b)^2)] & v_{t1} \leq v_{t2} + v_{t3}, 0 \leq \Delta\omega \leq \omega_1 \\ \frac{1}{v_{t1} v_{t2} v_{t3}} [b^2(v_{t1} v_{t2} + 3v_{t2} v_{t3} + v_{t3} v_{t1}) - b\Delta\omega(-v_{t1} + v_{t2} + v_{t3})] & \omega_1 \leq \Delta\omega \leq \omega_2 \\ -\frac{1}{2}(\Delta\omega^2 + (v_t b)^2) & \omega_1 \leq \Delta\omega \leq \omega_2 \\ \frac{2}{v_{t1} v_{t2}} [b^2(v_{t1} + v_{t2}) - v_t b \Delta\omega] & \omega_2 \leq \Delta\omega \leq \omega_3 \\ \frac{1}{2v_{t1} v_{t2} v_{t3}} [b(v_{t1} + v_{t2} + v_{t3}) - \Delta\omega]^2 & \omega_3 \leq \Delta\omega \leq \omega_4 \\ 0 & \Delta\omega \geq \omega_4 \end{cases} \quad (\text{A.4})$$

where $\Delta\omega = \omega - \omega_c$ and $v_t = |\mathbf{v}_t|$. $b = 1/(2N_1)$ is half side length of subcell of the transformed cubic region. Similarly, we assume that $\Delta\omega > 0$ and $v_{t1} \geq v_{t2} \geq v_{t3} \geq 0$, where $v_{ti} = \mathbf{v}_k \cdot \mathbf{b}_i$ is the component of transformed \mathbf{v}_t ($i = 1, 2, 3$). And $\omega_1 = b|v_{t1} - v_{t2} - v_{t3}|$, $\omega_2 = b(v_{t1} - v_{t2} + v_{t3})$, $\omega_3 = b(v_{t1} + v_{t2} - v_{t3})$, $\omega_4 = b(v_{t1} + v_{t2} + v_{t3})$.

The expressions of DOS calculation from one subcell (B.1) and (A.4) are equivalent. They only differ by a constant which is $dS_t/|\mathbf{v}_t| = \delta N/(8N_1 N_2 N_3)$.

Appendix B. GGR method in 2D

In order to use 3D GGR method for 2D lattices, we simply duplicate the frequency bands along a third imaginary dimension, so that the same GGR formulation applies with the following caveat.

In 3D, the DOS formula (A.4) is continuous (shown in figure 1 in [2]). However, for the extended 2D bands, the derivative of DOS is discontinuous due to $v_{t3} = 0$, $\omega_1 = \omega_2$ and $\omega_3 = \omega_4$. Thus, the 2D formula becomes,

$$\frac{dS_t}{|\mathbf{v}_t|} = \begin{cases} \frac{4b^2}{v_{t1}} & 0 \leq \Delta\omega \leq \omega_1 \\ \frac{2}{v_{t1} v_{t2}} [b^2(v_{t1} + v_{t2}) - v_t b \Delta\omega] & \omega_1 \leq \Delta\omega \leq \omega_3 \end{cases} \quad (\text{B.1})$$

whose first derivative is discontinuous at $\Delta\omega = \omega_1$. This discontinuity and the vanishing quadratic terms ($\Delta\omega^2$) lead to a zigzag DOS plot. The zigzag behavior also exists in tetrahedron method for the same reason, when being extended to 2D.

References

- [1] Andrew J Morris, Rebecca J Nicholls, Chris J Pickard, and Jonathan R Yates. Optados: A tool for obtaining density of states, core-level and optical spectra from electronic structure codes. *Computer Physics Communications*, 185(5):1477–1485, 2014.
- [2] G. Gilat and L. J. Raubenheimer. Accurate numerical method for calculating frequency-distribution functions in solids. *Physical Review*, 144(2):390–395, 1966.
- [3] L. J Raubenheimer and G Gilat. Accurate numerical method of calculating frequency distribution functions in solids. ii. extension to hcp crystals. *Physical Review*, 157(3):586–599, 1967.
- [4] Z Kam and G Gilat. Accurate numerical method for calculating frequency distribution functions in solids. iii. extension to tetragonal crystals. *Physical Review*, 175(3):1156, 1968.
- [5] E Finkman, Z Kam, E Cohen, and G Gilat. Accurate numerical method for calculating spectra in solids. iv. extension to trigonal crystals. *Journal of Physics and Chemistry of Solids*, 32(10):2423–2427, 1971.
- [6] H Bross. On the efficiency of different schemes for the evaluation of the density of states and related properties in solids. *physica status solidi (b)*, 179(2):429–439, 1993.
- [7] Jonathan R Yates, Xinjie Wang, David Vanderbilt, and Ivo Souza. Spectral and fermi surface properties from wannier interpolation. *Physical Review B*, 75(19):195121, 2007.
- [8] CJ Pickard and MC Payne. Extrapolative approaches to brillouin-zone integration. *Physical Review B*, 59(7):4685, 1999.
- [9] CJ Pickard and MC Payne. Second-order k p perturbation theory with vanderbilt pseudopotentials and plane waves. *Physical Review B*, 62(7):4383, 2000.
- [10] G Lehmann and M Taut. On the numerical calculation of the density of states and related properties. *physica status solidi (b)*, 54(2):469–477, 1972.
- [11] O Jepsen and OK Anderson. The electronic structure of hcp ytterbium. *Solid State Communications*, 9(20):1763–1767, 1971.
- [12] Peter E Blöchl, Ove Jepsen, and Ole Krogh Andersen. Improved tetrahedron method for brillouin-zone integrations. *Physical Review B*, 49(23):16223, 1994.
- [13] MS Methfessel, MH Boon, and FM Mueller. Analytic-quadratic method of calculating the density of states. *Journal of Physics C: Solid State Physics*, 16(27):L949, 1983.
- [14] MH Boon, MS Methfessel, and FM Mueller. Singular integrals over the brillouin zone: the analytic-quadratic method for the density of states. *Journal of Physics C: Solid State Physics*, 19(27):5337, 1986.
- [15] MS Methfessel, MH Boon, and FM Mueller. Singular integrals over the brillouin zone: inclusion of k-dependent matrix elements. *Journal of Physics C: Solid State Physics*, 20(8):1069, 1987.
- [16] Jorge E Müller and John W Wilkins. Band-structure approach to the x-ray spectra of metals. *Physical Review B*, 29(8):4331, 1984.
- [17] Kurt Busch and Sajeev John. Photonic band gap formation in certain self-organizing systems. *Physical Review E*, 58(3):3896, 1998.
- [18] Patrick M Johnson, A Femius Koenderink, and Willem L Vos. Ultrafast switching of photonic density of states in photonic crystals. *Physical Review B*, 66(8):081102, 2002.
- [19] Ivan S Nikolaev, Willem L Vos, and A Femius Koenderink. Accurate calculation of the local density of optical states in inverse-opal photonic crystals. *JOSA B*, 26(5):987–997, 2009.
- [20] P Kano, D Barker, and M Brio. Analysis of the analytic dispersion relation and density of states of a selected photonic crystal. *Journal of Physics D: Applied Physics*, 41(18):185106, 2008.
- [21] Victor Liu and Shanhui Fan. Efficient computation of equifrequency surfaces and density of states in photonic crystals using dirichlet-to-neumann maps. *JOSA B*, 28(8):1837–1843, 2011.
- [22] G Gilat. Analysis of methods for calculating spectral properties in solids. *Journal of Computational Physics*, 10(3):432–465, 1972.
- [23] G Wiesenekker and EJ Baerends. Quadratic integration over the three-dimensional brillouin zone. *Journal of Physics: Condensed Matter*, 3(35):6721, 1991.
- [24] Ling Lu, Liang Fu, John D Joannopoulos, and Marin Soljačić. Weyl points and line nodes in gyroid photonic crystals. *Nature photonics*, 7(4):294–299, 2013.
- [25] Luyang Wang, Shao-Kai Jian, and Hong Yao. Topological photonic crystal with equifrequency weyl points. *Physical Review A*, 93(6):061801, 2016.
- [26] Steven G. Johnson and J. D. Joannopoulos. Block-iterative frequency-domain methods for maxwell’s equations in a planewave basis. *Opt. Express*, 8(3):173–190, 2001.
- [27] R. I. Saye. High-order quadrature methods for implicitly defined surfaces and volumes in hyperrectangles. *Siam Journal on Scientific Computing*, 37(2):A993–A1019, 2015.